Journal of Theoretical Biology 528 (2021) 110839

Contents lists available at ScienceDirect

Journal of Theoretical Biology

journal homepage: www.elsevier.com/locate/yjtbi

Heterogeneity in susceptibility dictates the order of epidemic models

Christopher Rose [a], Andrew J. Medford [b], C. Franklin Goldsmith [a], Tejs Vegge [c], Joshua S. Weitz [d,*], Andrew A. Peterson [a,c,*]

[a] School of Engineering, Brown University, Providence, Rhode Island 02912, USA
[b] School of Chemical & Biomolecular Engineering, Georgia Institute of Technology, Atlanta, Georgia 30332, USA
[c] Department of Energy Conversion and Storage, Technical University of Denmark, Lyngby 2800 Kgs., Denmark
[d] School of Biological Sciences and School of Physics, Georgia Institute of Technology, Atlanta, Georgia 30332, USA

ARTICLE INFO

Article history:
Received 14 June 2021
Revised 16 July 2021
Accepted 18 July 2021
Available online 24 July 2021

Keyword:
Epidemiology
Nonlinear dynamics
Heterogeneity
Outbreaks
Forecasting

ABSTRACT

The fundamental models of epidemiology describe the progression of an infectious disease through a population using compartmentalized differential equations, but typically do not incorporate population-level heterogeneity in infection susceptibility. Here we combine a generalized analytical framework of contagion with computational models of epidemic dynamics to show that variation strongly influences the rate of infection, while the infection process simultaneously sculpts the susceptibility distribution. These joint dynamics influence the force of infection and are, in turn, influenced by the shape of the initial variability. We find that certain susceptibility distributions (the exponential and the gamma) are unchanged through the course of the outbreak, and lead naturally to power-law behavior in the force of infection; other distributions are often sculpted towards these "eigen-distributions" through the process of contagion. The power-law behavior fundamentally alters predictions of the long-term infection rate, and suggests that first-order epidemic models that are parameterized in the exponential-like phase may systematically and significantly over-estimate the final severity of the outbreak. In summary, our study suggests the need to examine the shape of susceptibility in natural populations as part of efforts to improve prediction models and to prioritize interventions that leverage heterogeneity to mitigate against spread.

© 2021 Elsevier Ltd. All rights reserved.

1. Introduction

Mathematical models of disease dynamics typically divide a population into categories based on infection status; *e.g.*, susceptible (S), infectious (I), and recovered/removed (R). In the basic SIR -model, the dynamics of individuals in each compartment can be written as Bjørnstad et al. (2020)

$$\frac{dS}{dt} = -r_{\mathrm{I}}$$
$$\frac{dI}{dt} = r_{\mathrm{I}} - r_{\mathrm{R}}, \qquad (1)$$

such that $S + I + R = 1$. The Kermack–McKendrick (Kermack and McKendrick, 1927) formulation—the basis for conventional, modern epidemiology models—assumes rates of infection and recovery to be $r_{\mathrm{I}} = \beta IS$ and $r_{\mathrm{R}} = \gamma I$, respectively, with β and γ taken as rate constants with dimensions of inverse time. These simplified models provide epidemiologists and policymakers with valuable intuition on the progression of an outbreak, and form the basis for more complex models that include such effects as geography, travel, latency (that is, a delay between exposure and infectiousness), susceptibility to re-infection, stochasticity, and vital dynamics (Anderson and May, 1992; Keeling and Rohani, 2007; Bertozzi et al., 2020; Moghadas et al., 2020). Previous studies have explored nonlinear forms for the rate of infection, r_{I}; many forms have been suggested including power laws and sub-exponential growth (Wilson and Worcester, 1945; Liu et al., 1986; Liu et al., 1987; Hethcote and van den Driessche, 1991; Regoes et al., 2002; Chowell et al., 2016).

The SIR model assumes homogeneity of risk, an assumption unlikely to hold in practice. That is, a real population will have a distribution of susceptibilities which can be based on a mixture of behavioral attributes (such as the number of people encountered in a typical day or interaction modalities) and inherent attributes (such as age, immune status, genetic differences, or varied responses to vaccines) (Longini and Halloran, 1996; Halloran et al., 1996; Woolhouse et al., 1997; Dwyer et al., 1997; Dwyer

* Corresponding authors.
E-mail addresses: jsweitz@gatech.edu (J.S. Weitz), andrew_peterson@brown.edu (A.A. Peterson).

https://doi.org/10.1016/j.jtbi.2021.110839
0022-5193/© 2021 Elsevier Ltd. All rights reserved.

et al., 2000; Smith et al., 2005; Izhar and Ben-Ami, 2015; King et al., 2018); additionally, a recent report has highlighted the need to understand the effect and sources of heterogeneity in disease spread as it pertains to the Covid-19 pandemic (Thompson et al., 2020). While measurement of susceptibilities is certainly not straightforward, studies suggest that for many diseases (including Covid-19) a small percentage of the population carries a majority of the population's total susceptibility (Corder et al., 2020; Dwyer et al., 1997; King et al., 2018; Smith et al., 2005; Endo et al., 2020; Wong and Collins, 2020).

If there is variation, then individuals that are more susceptible should tend to be infected earlier, leading to changes in the susceptibility distribution. As a result, the most susceptible individuals will be disproportionately removed from the pool at the early stages of an outbreak, so that not just the *number* of people in the susceptible pool will decrease, but also the *average susceptibility* of the pool will decrease, both of which should slow the rate of spread of infections. Here, we confine our analysis to the case where individuals have a static susceptibility over timescales relevant to an outbreak, noting that dynamic changes in behavior due to awareness of the outbreak can be accounted for separately (Funk et al., 2009; Eksin et al., 2019; Weitz et al., 2020). In the conclusions, we also discuss the potential impacts of heterogeneity in infectiousness and correlations between susceptibility and infectiousness on disease spread. Our framework assigns variation in susceptibility to individuals, rather than events. We note that the incidence of super-spreading events (linked to "super-spreaders") may be driven in part by behavioral differences, suggesting that control and mitigation efforts could focus on reducing situational risk in addition to identification of intrinsic, individual-associated variation (Chande et al., 2020; Sneppen et al., 2021; Kain et al., 2021).

One way to incorporate variability into the SIR model is to directly account for susceptibility in the rate equations. Other epidemic models have incorporated such variability by explicitly accounting for assortative mixing (Britton et al., 2020) or variation in contacts (Hébert-Dufresne et al., 2020), by implicitly structuring a population based on variation in susceptibility (Gomes et al., 2020), or by the use of network-based models (Bansal et al., 2007). These analyses make different assumptions about the link between variation in risk and infection dynamics. Despite the use of different assumptions, all of these models suggest that variation in the risk of transmission can lower the herd immunity threshold (*i.e.*, the fraction of the population that must become immune for the disease to decrease in prevalence) when compared to predictions from equivalent homogeneous mixing models. This agreement suggests it may be possible to develop a unified framework to understand the joint dynamics of infection and susceptibility. In this work, we develop simple and computationally efficient means to rigorously account for heterogeneity within compartmentalized models.

2. The effect of heterogeneity on dynamics

First, we define an individual's infection susceptibility, ε, such that individuals with $\varepsilon = 2$ will become infected at twice the rate, on average, as individuals with $\varepsilon = 1$, given they exist in the same population of infected people. This definition is generic, and captures heterogeneity due to behavioral and/or inherent factors, such as those listed earlier. If the distribution of susceptibilities in a pop-

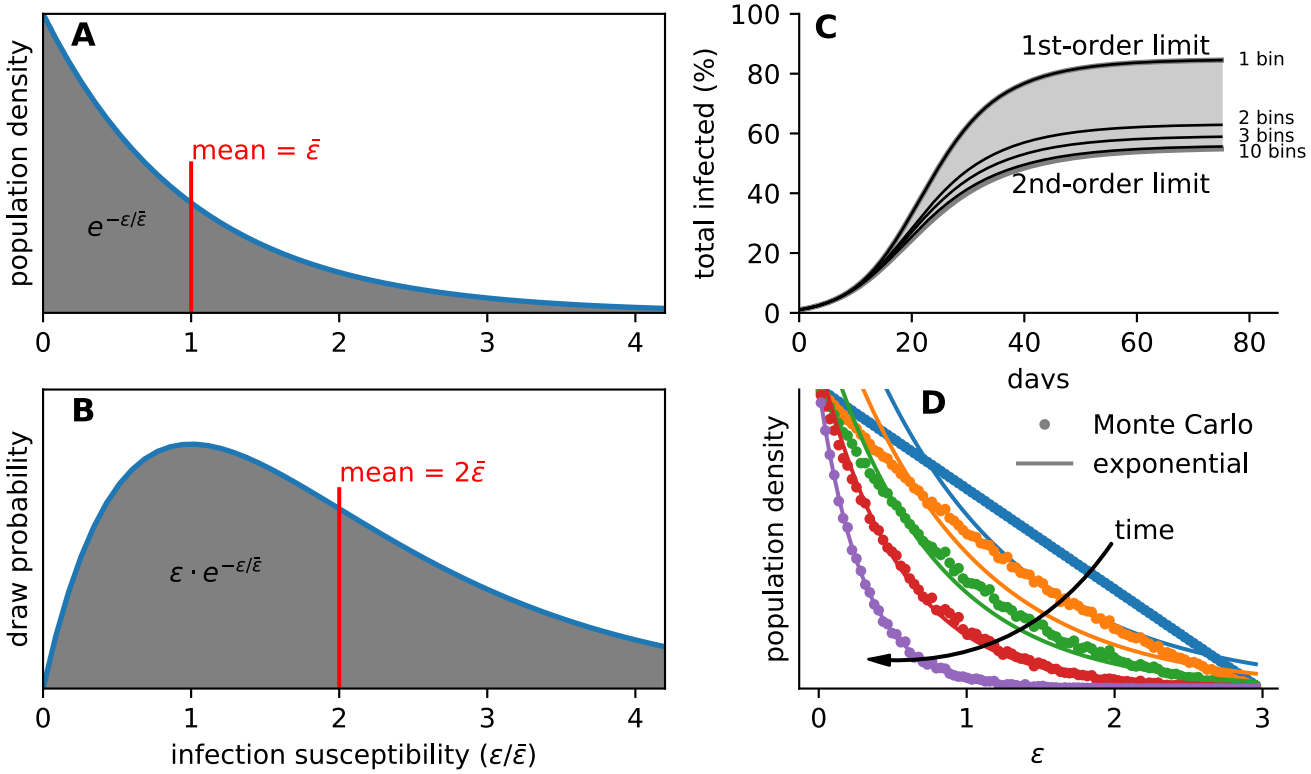


Fig. 1. A and B show a continuous distribution of infection susceptibility in a population and the probability of the next individual infected, respectively. For an exponential distribution, the mean of the lower curve is double the mean of the upper curve. **C** compares numerically integrating a 1st- and 2nd-order SIR model with that obtained from binning the susceptibility into discrete levels consistent with an initially-exponential distribution. **D** shows that an exponential distribution emerges when stochastically sampling from an initially linear distribution. The solid lines are exponential curves with the same mean as the Monte Carlo points of the same color.

ulation is given by $n_S(\varepsilon,t)$ (which we show for the example of an exponential distribution in Fig. 1A); then the infection rate is distributed as

$$\hat{r}_I(\varepsilon,t) = \beta I \varepsilon \frac{n_S(\varepsilon,t)}{N_{total}} \propto \varepsilon \cdot n_S(\varepsilon,t), \tag{2}$$

where N_{total} is the total number of individuals in the population. This distribution, which we refer to as the "draw probability" —that is, the conditional probability that a just-infected individual has susceptibility ε—is shown in Fig. 1B, where it is apparent that the mean of the draw probability is higher than the mean of the susceptible pool. This will be true of *any* (non-singular) population distribution, putting downward pressure on the mean. The overall rate of new infections at any time is then

$$\begin{aligned} r_I &= \int_0^\infty \beta I \varepsilon \, \tfrac{n_S(\varepsilon,t)}{N_{total}} \, d\varepsilon \\ r_I &= \beta I \bar{\varepsilon} S \quad \text{(any distribution)}, \end{aligned} \tag{3}$$

where $\bar{\varepsilon}(t)$ is the mean susceptibility of the pool, since $\bar{\varepsilon}(t) = \frac{1}{N_S}\int_0^\infty \varepsilon n_S(\varepsilon,t)\,d\varepsilon$ with N_S as the total number of susceptible people in the population. This rate form ($\beta\bar{\varepsilon}IS$) is general; for example, if the entire population has an identical susceptibility of $\varepsilon = 1$, (3) simplifies to the classic SIR rate.

In principle, the only constraints on values of ε in $n_S(\varepsilon,t)$ are that $\varepsilon \geqslant 0$ and that $\bar{\varepsilon}$ is finite; a natural starting point is to assume that susceptibility follows the maximum-entropy distribution (*i.e.*, the least-informative default) under these constraints, which for positive values with a specified mean is the exponential distribution (Jaynes, 2003)

$$\frac{n_S(\varepsilon,t)}{N_S} = \frac{e^{-\varepsilon/\bar{\varepsilon}(t)}}{\bar{\varepsilon}(t)}.$$

For this distribution, the draw probability has a mean value of $2\bar{\varepsilon}(t)$ (at any time, provided the distribution remains exponential); that is, the average individual who has just gotten infected was twice as susceptible as the susceptible population as a whole. (All derivations and assumptions not explicitly detailed in this manuscript are contained in the SI.) We can then express how the population's average susceptibility $\bar{\varepsilon}$ is affected by the removal of high-ε individuals. Since, on average, the susceptibility of a newly infected individual is $2\bar{\varepsilon}$, the population's total susceptibility decreases as $d(\bar{\varepsilon}N_S)/dN_S = 2\bar{\varepsilon}$. Upon integration, we find the *average* susceptibility of the population decreases in direct proportion to the number of individuals left in the subpopulation of susceptibles:

$$\bar{\varepsilon}(t) = S(t) \quad \text{(exponential dist.)}, \tag{4}$$

(where, without loss of generality, we define the initial population to have $\bar{\varepsilon} = 1$). As a result, the rate of new infections (from (3)) becomes second order in S,

$$r_I = \beta I S^2 \quad \text{(exponential dist.)}.$$

A similar result should be observed by "binning" the susceptibility into discrete levels and introducing a separate ODE for each susceptibility level, as has been employed in previous literature (Langwig et al., 2017; King et al., 2018); the match should improve as the number of bins increases, becoming exact at infinite binning. We show the results of numerically integrating such a binned system given an initially exponential susceptibility distribution in Fig. 1C. As the number of discrete susceptibility levels is increased, we approach the second-order behavior predicted by this analysis.

3. The sculpting of susceptibility distributions by disease spread

The above analysis holds if the distribution is expected to remain exponential throughout the course of the outbreak. Since a distribution will evolve as $\partial n_S(\varepsilon,t)/\partial t = -\beta I \varepsilon n_S(\varepsilon,t)$, then the time-course of the distribution will follow

$$n_S(\varepsilon,t) = n_S(\varepsilon,0) \cdot e^{-\varepsilon\phi(t)}, \tag{5}$$

where $n_S(\varepsilon,0)$ is the initial distribution and $\phi(t) \equiv \beta\int_0^t I dt$ is a dimensionless progress variable that is monotonic with time. $\phi(t)$ can be thought of as the cumulative infectious driving force. Therefore, an initially exponential distribution will evolve as

$$n_S(\varepsilon,t) = \frac{N_{total}}{\bar{\varepsilon}_0} \exp\left\{-\left(\frac{1}{\bar{\varepsilon}_0} + \phi(t)\right)\cdot\varepsilon\right\},$$

where $\bar{\varepsilon}_0$ is the initial mean. That is, the distribution stays exponential with respect to ε at all times, validating the continued use of the exponential distribution in (4).

Interestingly, we also find that many starting distributions evolve toward an exponential form under the action of contagion. This is shown for a linearly-decreasing distribution in Fig. 1D, which we observed via Monte Carlo simulations to tend towards an exponential, through a stochastic sampling process consistent with the draw probability. Indeed, this sculpting behavior can be inferred from (5), which for an initially linearly-decreasing distribution is proportional to $(\varepsilon_{max} - \varepsilon)\cdot\exp\{-\phi(t)\varepsilon\}$, where the exponential term becomes dominant as $\phi(t)$ increases.

We can use (5) to describe how contagion sculpts any arbitrary susceptibility distribution. For convenience, we employ the beta distribution, which allows us to craft distributions of characteristic initial shapes, and in Fig. 2 we use this distribution to create initial distributions that are longer-tailed (A), bimodal (B), uniform (C), and unimodal (D). Here, we can clearly see how the process of contagion sculpts distributions; features with large ε are quickly diminished; that is, the individuals with high susceptibility to infection are preferentially removed from $n_S(\varepsilon,t)$ at early times. In these sculpting plots, we also show a gamma distribution for reference, with its shape parameter k equal to the a parameter of the beta distribution, and we see that the contagion process sculpts these distributions towards their gamma counterparts. Parts E–H of this figure show the sculpting of gamma distributions, which we see retain their shape during the act of contagion. Indeed, it can be derived that any well-behaved initial distribution—specifically one that is continuous and can be expressed as a power series at its leftmost extent—will approach a gamma distribution under the sculpting process of (5); we show this in SI Section S3.3, which also links the beta's a parameter to the gamma's k parameter. After a more detailed analysis of the gamma distribution, we will show how the initial distribution shape and the sculpting process interact with the outbreak dynamics.

The gamma distribution is often used to describe variations in susceptibility (Dwyer et al., 1997; Smith et al., 2005; Langwig et al., 2017; King et al., 2018). This distribution,

$$\frac{n_S(\varepsilon,0)}{N_{total}} = \frac{\varepsilon^{k-1}e^{-\varepsilon k/\bar{\varepsilon}_0}}{\left(\frac{\bar{\varepsilon}_0}{k}\right)^k \Gamma(k)},$$

is controlled via a shape parameter k and simplifies to the exponential when $k = 1$. If $k < 1$, the gamma becomes a longer-tailed distribution (such as an "80:20" distribution at $k \cong 0.25$, where 80% of the variation is captured by the most susceptible 20% of the population), and as $k \to \infty$ the distribution becomes a Dirac delta function. For many diseases (including SARS-CoV-2), k has been reported to be less than one (Dwyer et al., 1997; Smith et al., 2005; Gomes et al., 2020; Corder et al., 2020). As we observed in

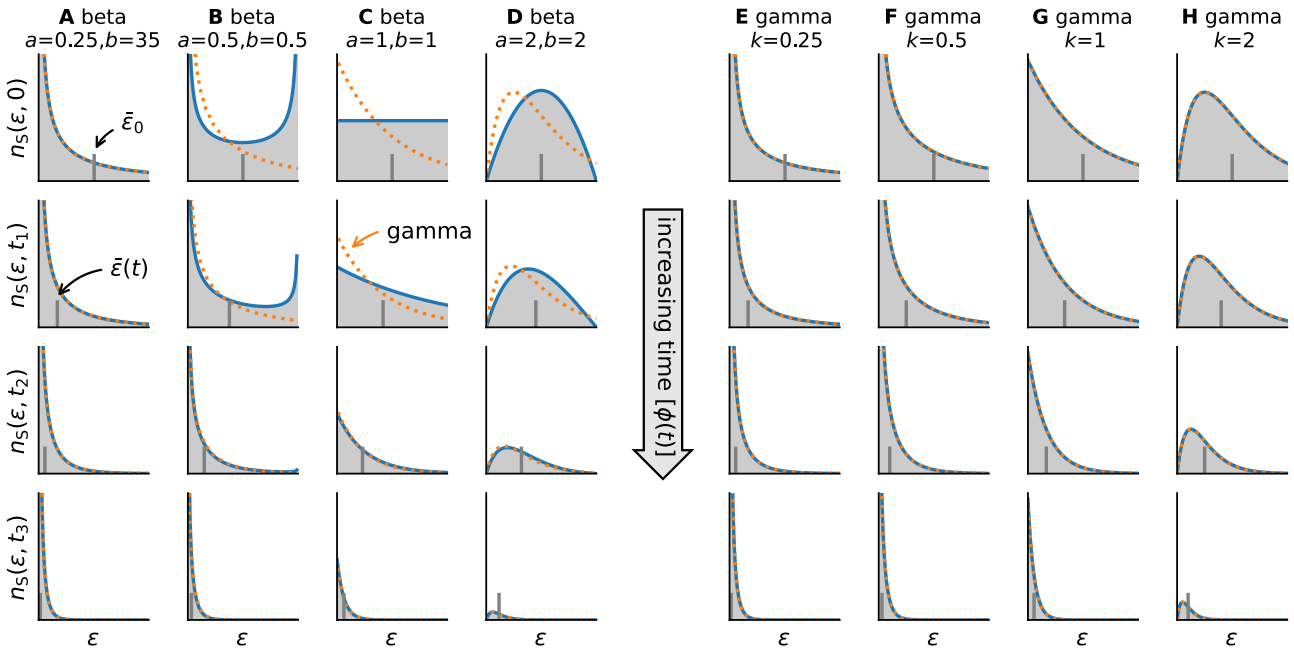


Fig. 2. The sculpting of susceptibility distributions under the act of contagion; that is, by (5). Each column represents the initial distribution indicated at the top of that column, with the shape of that distribution changing with increasing time (tracked by $\phi(t)$) proceeding down the column; at values of $\phi(t) = 0, \frac{1}{2}, 2$, and 4. In A–D, the orange dashed line shows a gamma function with the same mean and shape parameter $k = a$; in E–H the orange line is included to emphasize that a gamma distribution retains its shape. The small vertical bars indicate $\bar{\varepsilon}$, which is set to 1 in all $t = 0$ plots. All plots are scaled identically; that is, all share the same limits on both the abscissa and ordinate.

Fig. 2 and formalize in SI Section S3.2.2, the gamma distribution is a general solution to the differential equation governing the dynamic sampling process; this makes it an "eigen-distribution" of the force of infection. (The Gaussian distribution may also act as an eigen-distribution but is of less practical use, as we discuss in SI Section S6.) That is, if a population is initially gamma-distributed it will remain gamma-distributed—with the same shape parameter k and decreasing mean—under the action of (5).

4. General power-law behavior

It is straightforward to derive (SI Section S1.3) that the mean susceptibility, for any given initial distribution, changes as

$$\frac{d\bar{\varepsilon}}{dS} = \frac{\sigma^2}{\bar{\varepsilon} S} \quad \text{(any distribution)}$$

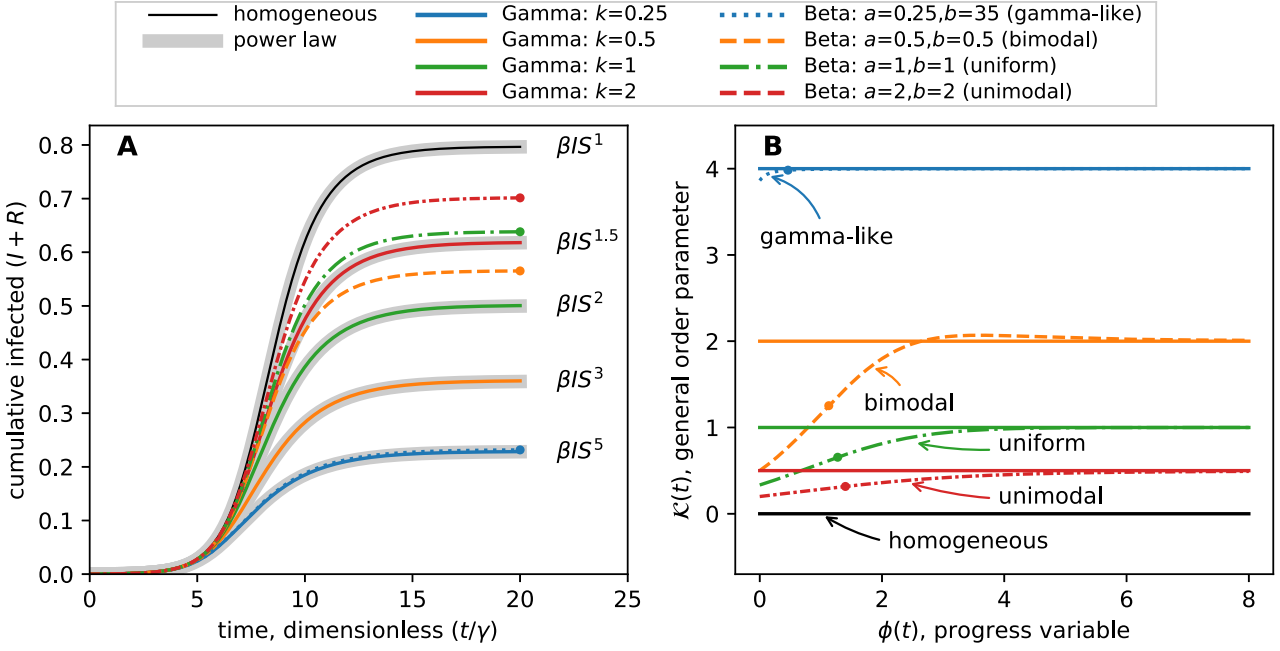


Fig. 3. How the initial susceptibility distribution affects the joint dynamics of infection and distribution sculpting. **A** Infection dynamics for the distributions shown in Fig. 2. The gray background curves show power-law models (βIS^p) for comparisons. Time is non-dimensionalized by the recovery rate constant. **B** Effective order parameter $\mathcal{K}(t)$ for the same distributions. For the gamma distribution, the order is always $1/k$; for the beta distributions, the order approaches that of a gamma distribution as the sculpting process proceeds. The dot on each beta curve indicates the value at $t/\gamma = 20$. The legend applies to both **A** and **B**.

where $\sigma^2(t)$ is the variance of the distribution. Since the variance of the gamma function is $\sigma^2(t) = \bar{\varepsilon}(t)^2/k$ and k stays constant during contagion, it follows that the mean susceptibility scales as

$$\bar{\varepsilon} = S^{1/k} \quad \text{(gamma dist.)}$$

for an initial outbreak, giving a rate

$$r_1 = \beta I S^{1+\frac{1}{k}} \quad \text{(gamma dist.)}.$$

This is exact power-law behavior for gamma-distributed susceptibilities, where the power is given by $p = 1 + 1/k$. Such power-law behavior has been previously derived for gamma distributions (Novozhilov, 2008a,b; Novozhilov, 2012; Karev and Novozhilov, 2019); here we also show how distributions develop over time and that the gamma distribution can often be considered an attractor distribution. Elsewhere, power-law behavior has been suggested for models of behavioral change (Eksin et al., 2019); here, the behavior emerges naturally from the distribution. In the case of exponentially-distributed susceptibility ($k = 1$), second-order behavior emerges. A longer tail, corresponding to small values of k, can significantly increase the power; for example, the "80:20" distribution ($k \approx 0.25$) pushes the order to approximately five. It is only in the unlikely limit that all individuals are identical ($k \to \infty$) that we recover the first-order power of the classic SIR -model, suggesting the standard SIR model relies on an extreme assumption about variation in susceptibility. This power law provides a convenient framework for capturing the effects of heterogeneous susceptibility through a single additional power-law parameter, which is dictated by the variability of susceptibility.

Next we show how the sculpting process and the outbreak dynamics interact, allowing us to understand how the initial shape of the susceptibility distribution affects the dynamics of disease spread. Conventionally, when outbreak models (*e.g.*, the SIR) are analyzed they are numerically integrated, and when differences in susceptibility are desired this can be achieved by "binning" the susceptibility into many discrete histogram bins (Langwig et al., 2017; King et al., 2018), as we did in Fig. 1C. However, it is straightforward to track the cumulative progress of the epidemic $\phi(t)$ during the numerical integration. Insofar as we can analytically express the mean susceptibility time course $\bar{\varepsilon}(\phi(t))$ for a given initial distribution under the action of (5), we can model outbreak dynamics for arbitrary initial distributions without resorting to the computational expense or complexity involved with binning. We give full details of how this can be simply implemented in SI Section S4. We note that methods have been introduced in prior literature to integrate such a system without binning, notably a method that approximates the partial differential equation as a truncated set of ordinary differential equations involving the moments of the distribution, making subsequent assumptions about relationships between these moments (Dushoff, 1999; Dwyer et al., 1997). In contrast, the method here gives an exact solution, shows precisely when assumptions about moment relationships hold, and does so without expanding the number of differential equations, relative to the standard SIR model. We have performed this integration for the initial distributions shown in Fig. 2, and the results are shown in Fig. 3A. Here, we see an orderly progression among the gamma distributions, with the longer-tailed distributions exhibiting reduced final outbreak size; further, we see that the gamma and beta distributions whose initial shape is nearly indistinguishable (gamma, $k = 0.25$ with beta, $a = 0.25, b = 35$) behave almost indistinguishably. As expected, the gamma distributions follow the power-law relations exactly. As is apparent, the longer the tail on the distribution, the more suppressed the size of the outbreak, as the initially high rate is caused by those with abnormally high susceptibilities.

While we have only analytically derived a power law for gamma distributions, relating $\bar{\varepsilon}$ to S^p, for other distributions we can define an instantaneous order parameter $\mathscr{K}(t)$ as

$$\mathscr{K}(t) \equiv \frac{d(\ln \bar{\varepsilon})}{d(\ln S)}$$

which allows us to understand the deviation from such a law, and can inform us how the contagion process sculpts the susceptibility distribution. For gamma distributions, $\mathscr{K}(t) = 1/k$ at all times. We provide an expression for $\mathscr{K}(t)$ in terms of $\phi(t)$ for the beta distribution in SI Section S3.2.3, and in Fig. 3B we show how $\mathscr{K}(t)$ changes for the beta distributions. We see that instantaneous orders of the beta distributions tend towards the orders of the corresponding gamma distributions. That is, the contagion process sculpts the beta distributions towards gamma distributions, and as this happens the order approaches the constant order of the gamma distribution. How this affects the outbreak behavior depends upon the relevant timescales of the sculpting process versus that of the infection dynamics.

For the beta distribution at $a = \frac{1}{4}, b = 35$, which very closely resembles a gamma distribution, we see that the order starts at approximately 4 and closely follows the behavior of the corresponding ($k = 4$) gamma distribution. This was also apparent from the numerical integration of these two starting distributions, which give nearly indistinguishable results. That is, if the initial distribution can be reasonably approximated by a gamma distribution, then we can expect the power-law behavior to describe well the dynamics. For the more extreme initial distributions, such as the bimodal or uniform, we see that $\mathscr{K}(t)$ changes much more dramatically over the course of the outbreak. Although they approach a gamma distribution at large values of $\phi(t)$, in practice these $\phi(t)$ values may never be reached, as the outbreak may reach its final size before the sculpting process can asymptote. We see precisely this for the bimodal and uniform distributions, where the dot on the $\mathscr{K}(t)$ figures shows the value of $\mathscr{K}(t)$ at a time when the epidemic has, in effect, concluded. Finally, we see the unimodal distribution has a relatively low order parameter, which we expect, as this most closely resembles the implied homogeneous assumption of the classic SIR model, for which $\mathscr{K}(t) = 0$ at all times.

5. Effects on epidemic model predictions

How does a power-law dependence of the infection rate affect epidemic model predictions? First, we note that in the early, exponential-like growth phase of an outbreak—when most of the pre-emptive measures are decided—the models are indistinguishable (since $S \approx 1$, then $S^p \approx 1$). This means that when the model parameters are fit in this exponential-like growth phase, the estimate of β (or alternatively $\mathscr{R}_0 \equiv \beta/\gamma$) will be identical in each model (see Fig. 4A). A deviation in the dynamics of the different models appears given sufficient depletion of susceptibles (see Fig. 4B). Assuming the epidemic proceeds in a naïve population, the final size under a 2nd-order model is predicted to be

$$Z = 1 - \frac{1}{\mathscr{R}_0} \quad \text{(2nd order)}.$$

For 1st- and pth-orders, implicit algebraic equations are given in SI Section S5. Fig. 4B shows that there can be very substantial differences between final size predictions when comparing the conventional SIR model with predictions from models with intrinsic variation in susceptibility. We note that these results agree with predictions made elsewhere that heterogeneity reduces the predicted severity of the outbreak (Eksin et al., 2019; Gomes et al.,

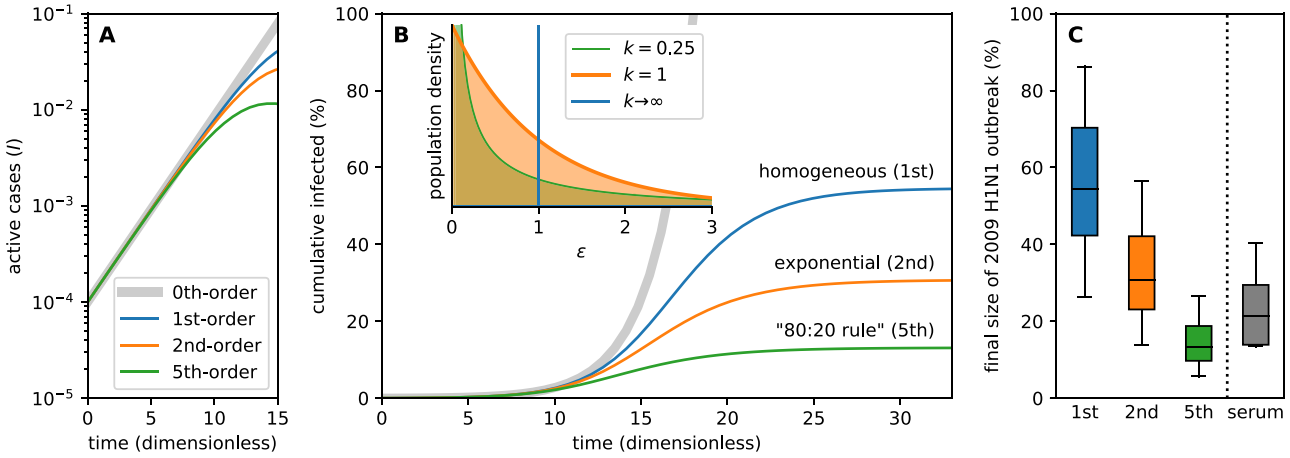


Fig. 4. Outbreak dynamics and model comparison to the 2009 H1N1 outbreak. **A**: The higher-order models are indistinguishable from one another in the early, exponential-like region (marked as "0th-order"), where the models are frequently parameterized. **B**: Outbreak progression with various assumed susceptibility distributions. The inset shows a gamma distribution at different k values. In all models, $\beta/\gamma(=\mathscr{R}_0)$ is set to 1.47, the median value estimated from 78 studies at the early stages of the 2009 H1N1 outbreak, (Biggerstaff et al., 2014) and time is non-dimensionalized by the recovery rate ($\gamma \cdot t$). **C**: Final size predictions based on the 78 R_0 values measured (Biggerstaff et al., 2014) at early stages of the infection, in the 1st-, and 2nd-, and 5th-order models, compared with 11 seroepidemiological measurements obtained (Nishiura et al., 2011) after the outbreak stabilized.

2020; Britton et al., 2020; Hébert-Dufresne et al., 2020). Within the power-law model, the herd-immunity threshold is predicted to be

$$p_c = 1 - \frac{1}{\mathscr{R}_0^{1/p}}.$$

These herd-immunity and final-size analyses are only meaningful when the population's immunity is accrued naturally through the dynamics of the outbreak itself; if immunity is acquired through vaccinations applied randomly, then the final-size and herd-immunity estimates will tend toward the classic SIR predictions.

Differences in final-size predictions when including risk heterogeneity as compared to those from conventional SIR models can be relevant to real-world outbreaks, as we examine for the 2009 H1N1 influenza outbreak, where initial estimates of the final outbreak size were reportedly much higher than occurred in practice (Nishiura et al., 2011). In Fig. 4B, we compare the power-law behavior using models parameterized with the mean $\mathscr{R}_0$ estimated at the early stages of the outbreak (Nishiura et al., 2011). In the included bar chart (Fig. 4C), we compare model predictions using 78 published estimates of $\mathscr{R}_0$ (from different locales) (Biggerstaff et al., 2014) to final-size measurements based on 11 serological studies (Nishiura et al., 2011). We observe that the higher-order models are more consistent with the final-size measurements. It is not uncommon for models to over-predict the ultimate size of epidemics (Butler, 2014; King et al., 2015; Nishiura et al., 2011), although we note that non-pharmaceutical interventions such as social distancing are expected to reduce this final size (Ma and Earn, 2006; Bjørnstad et al., 2020), even after being later relaxed. While predicting final outbreak sizes based on initial measurements is challenging, the significant improvement of the higher-order models lends credence to the importance of accounting for heterogeneity in the susceptibility of naïve populations.

6. Conclusions

Here, we have shown how heterogeneity in susceptibility affects disease spread, and how the infection process itself sculpts the distribution of susceptible individuals. The central conclusions of this study are as follows:

1. The presence of heterogeneity in susceptibility will always act to decrease the size of an outbreak, as compared to SIR model predictions. Heterogeneity decreases outbreak size because the most susceptible individuals are preferentially infected and removed from the population of susceptibles earlier in the outbreak. The dynamics of disease spread in heterogeneous populations implies that there is a decrease in both the *number* of susceptible individuals and the *average* susceptibility of the subpopulation that is still susceptible to the disease.
2. A gamma distribution is a natural choice to account for variations in susceptibility, as it is an "eigen-distribution" of the sculpting process of infection; that is, an initially gamma-distributed population stays gamma-distributed with shape parameter k and decreasing mean. Additionally, the gamma often serves as an attractor; that is, other distributions are frequently sculpted towards gamma-shaped distributions.
3. When heterogeneity can be well-described by a gamma distribution with shape parameter k, the rate form simplifies to a power law; that is, $\beta I S^p$, where $p = 1 + 1/k$.
4. If nothing is known about the distribution of susceptibility for a particular disease, a natural first choice is the exponential distribution (which is the maximum-entropy distribution bounded in $(0, \infty)$ with a specified initial mean). Since the exponential distribution is equivalent to a gamma distribution with $k = 1$, the resulting dynamics are second-order ($\beta I S^2$).
5. Other distributions can be used to describe the initial susceptibility and run through SIR models with minimal computational complexity or expense, and without resorting to binning the susceptibility into compartments. This is accomplished by using the general rate form ($\beta I \bar{\varepsilon} S$) and tracking how $\bar{\varepsilon}(t)$ follows $\phi(t)$, which can be readily derived for most distributions. $\phi(t)$, a dimensionless progress variable, is proportional to $R(t)$ in the SIR model. See SI Section S4.

There are other factors worth considering in this analysis. First, this framework does not assume any correlation between spreading propensity and infection susceptibility, so that super-spreaders appear with a frequency identical to their prevalence in the population. It seems plausible that many of the social traits that contribute to higher susceptibility would also lead to higher spreading. If a positive correlation exists between spreading and susceptibility, then the "super-spreaders" will be most active at

the beginning of an outbreak and contribute disproportionately to the rate of infection, but as the outbreak progresses, they also will be disproportionately removed early, causing more downward pressure on the relative rate of infection. The impact of such correlations would benefit from further study. Our analysis also assumes that the susceptibility of each individual in the population is static over the timescales relevant to the outbreak, so that an individual does not become more or less susceptible at any point, and that there is no societal response. If these changes to susceptibility are random, this would decrease the effect suggested here; however, behavior responses may increase the effect (Funk et al., 2009; Eksin et al., 2019; Weitz et al., 2020).

Critically, the analysis provided here reveals that assessing the joint dynamics of the susceptibility distribution can have drastic consequences on naturally-acquired herd immunity predictions, highlighting the importance of quantifying susceptibility variance for infectious diseases. In addition, characterizing heterogeneity in populations and identifying drivers of greater susceptibility may also help prioritize interventions that aim to decrease the risk of infection to those most likely to be infected and infect others (*e.g.*, see (Nielsen et al., 2021; Kain et al., 2021)). Although heterogeneity means that some individuals can disproportionately drive transmission, characterizing this variation can also constitute the basis for targeted interventions.

Supporting information. Detailed derivations and assumptions are provided in the Supporting Information (SI) for all concepts presented in this work; references in this work to sections in the SI begin with "S". The SI includes derivations of the general rate form, the sculpting of distributions by contagion, the emergence of higher-order kinetics, the instantaneous order parameter, as well as final-size and herd-immunity calculations. Full details on how SIR-type models with arbitrary initial distributions can be integrated without expanding the size of the set of differential equations are also provided. Finally, a critical discussion of the use of the Gaussian distribution to describe variations in susceptibility is presented.

Declaration of Competing Interest

The authors declare that they have no known competing financial interests or personal relationships that could have appeared to influence the work reported in this paper.

Acknowledgment

The authors are grateful to Johnny Guzman (Brown University) for useful discussions on eigenfunction uniqueness proofs.

Appendix A. Supplementary data

Supplementary data associated with this article can be found, in the online version, at https://doi.org/10.1016/j.jtbi.2021.110839.

References

Anderson, R.M., May, R.M., 1992. Infectious Diseases of Humans: Dynamics and Control. Oxford University Press.
Bansal, S., Grenfell, B.T., Ancel Meyers, L., 2007. When individual behaviour matters: homogeneous and network models in epidemiology. J. R. Soc. Interf. 4, 879–891.
Bertozzi, A.L., Franco, E., Mohler, G., Short, M.B., Sledge, D., 2020. The challenges of modeling and forecasting the spread of COVID-19. Proc. Nat. Acad. Sci. USA 117, 16732–16738.
Biggerstaff, M., Cauchemez, S., Reed, C., Gambhir, M., Finelli, L., 2014. Estimates of the reproduction number for seasonal, pandemic, and zoonotic influenza: a systematic review of the literature. BMC Infect. Dis. 14, 480.
Bjørnstad, O.N., Shea, K., Krzywinski, M., Altman, N., 2020. Modeling infectious epidemics. Nat. Methods 17, 455–456.
Britton, T., Ball, F., Trapman, P., 2020. A mathematical model reveals the influence of population heterogeneity on herd immunity to SARS-CoV-2. Science 369, 846–849.
Butler, D., 2014. Models overestimate Ebola cases. Nature 515, 18.
Chande, A., Lee, S., Harris, M., Nguyen, Q., Beckett, S.J., Hilley, T., Andris, C., Weitz, J. S., 2020. Real-time, interactive website for US-county-level COVID-19 event risk assessment. Nat. Human Behav. 4, 1313–1319.
Chowell, G., Sattenspiel, L., Bansal, S., Viboud, C., 2016. Mathematical models to characterize early epidemic growth: A review. Phys. Life Rev. 18, 66–97.
Corder, R.M., Ferreira, M.U., Gomes, M.G.M., 2020. Modelling the epidemiology of residual Plasmodium vivax malaria in a heterogeneous host population: A case study in the Amazon Basin. PLoS Comput. Biol. 16, e1007377.
Dushoff, J., 1999. Host heterogeneity and disease endemicity: a moment-based approach. Theor. Popul. Biol. 56, 325–335.
Dwyer, G., Elkinton, J.S., Buonaccorsi, J.P., 1997. Host heterogeneity in susceptibility and disease dynamics: tests of a mathematical model. Am. Nat. 150, 685–707.
Dwyer, G., Dushoff, J., Elkinton, J.S., Levin, S.A., 2000. Pathogen-driven outbreaks in forest defoliators revisited: building models from experimental data. Am. Nat. 156, 105–120.
Eksin, C., Paarporn, K., Weitz, J.S., 2019. Systematic biases in disease forecasting – The role of behavior change. Epidemics 27, 96–105.
Endo, A., Abbott, S., Kucharski, A.J., S.F., 2020. Estimating the overdispersion in COVID-19 transmission using outbreak sizes outside China. Welcome Open Res. 5, 67..
Funk, S., Gilad, E., Watkins, C., Jansen, V.A.A., 2009. The spread of awareness and its impact on epidemic outbreaks. Proc. Nat. Acad. Sci. 106, 6872–6877.
Gomes, M.G.M., Corder, R.M., King, J.G., Langwig, K.E., Souto-Maior, C., Carneiro, J., Goncalves, G., Penha-Goncalves, C., Ferreira, M.U., Aguas, R., 2020. Individual variation in susceptibility or exposure to SARS-CoV-2 lowers the herd immunity threshold. medRxiv 2020.04.27.20081893..
Halloran, M.E., Longini, I.M., Struchiner, C.J., 1996. Estimability and interpretation of vaccine efficacy using frailty mixing models. Am. J. Epidemiol. 144, 83–97.
Hébert-Dufresne, L., Althouse, B.M., Scarpino, S.V., Allard, A., 2020. Beyond R_0: Heterogeneity in secondary infections and probabilistic epidemic forecasting. ArXiV 2020; 2002.04004..
Hethcote, H.W., van den Driessche, P., 1991. Some epidemiological models with nonlinear incidence. J. Math. Biol. 29, 271–287.
Izhar, R., Ben-Ami, F., 2015. Host age modulates parasite infectivity, virulence and reproduction. J. Anim. Ecol. 84, 1018–1028.
Jaynes, E.T., 2003. Probability Theory. Cambridge University Press.
Kain, M.P., Childs, M.L., Becker, A.D., Mordecai, E.A., 2021. Chopping the tail: How preventing superspreading can help to maintain COVID-19 control. Epidemics 34, 100430.
Karev, G.P., Novozhilov, A.S., 2019. How trait distributions evolve in populations with parametric heterogeneity. Math. Biosci. 315, 108235.
Keeling, M.J., Rohani, P., 2007. Modeling Infectious Diseases in Humans and Animals. Princeton University Press. 1st Ed..
Kermack, W.O., McKendrick, A.G., 1927. A contribution to the mathematical theory of epidemics. Proc. R. Soc. London. A 115, 700–721.
King, A.A., de Cellès, M.D., Magpantay, F.M.G., Rohani, P., 2015. Avoidable errors in the modelling of outbreaks of emerging pathogens, with special reference to Ebola. Proc. R. Soc. B 282, 20150347.
King, J.G., Souto-Maior, C., Sartori, L.M., de Freitas, R.M., Gomes, M.G.M., 2018. Variation in Wolbachia effects on Aedes mosquitoes as a determinant of invasiveness and vectorial capacity. Nat. Commun. 9, 1483.
Langwig, K.E., Wargo, A.R., Jones, D.R., Viss, J.R., Rutan, B.J., Egan, N.A., Sá-Guimarães, P., Kim, M.S., Kurath, G., Gomes, M.G.M., Lipsitch, M., 2017. Vaccine Effects on Heterogeneity in Susceptibility and Implications for Population Health Management. mBio 2017; 8, e00796-17..
Liu, W., Levin, S.A., Iwasa, Y., 1986. Influence of nonlinear incidence rates upon the behavior of SIRS epidemiological models. J. Math. Biol. 23, 187–204.
Liu, W., Hethcote, H.W., Levin, S.A., 1987. Dynamical behavior of epidemiological models with nonlinear incidence rates. J. Math. Biol. 25, 359–380.
Longini, I.M., Halloran, M.E., 1996. A frailty mixture model for estimating vaccine efficacy. Appl. Stat. 45, 165.
Ma, J., Earn, D.J.D., 2006. Generality of the final size formula for an epidemic of a newly invading infectious disease. Bull. Math. Biol. 68, 679–702.
Moghadas, S.M., Fitzpatrick, M.C., Sah, P., Pandey, A., Shoukat, A., Singer, B.H., Galvani, A.P., 2020. The implications of silent transmission for the control of COVID-19 outbreaks. Proc. Nat. Acad. Sci. USA 117, 17513–17515.
Nielsen, B.F., Simonsen, L., Sneppen, K., 2021. COVID-19 superspreading suggests mitigation by social network modulation. Phys. Rev. Lett. 126.
Nishiura, H., Chowell, G., Castillo-Chavez, C., 2011. Did modeling overestimate the transmission potential of pandemic (H1N1-2009)? sample size estimation for post-epidemic seroepidemiological studies. PLoS ONE 6, e17908.
Novozhilov, A.S., 2008a. On the spread of epidemics in a closed heterogeneous population. Math. Biosci. 215, 177–185.
Novozhilov, A.S., 2008. Heterogeneous Susceptibles-Infectives model: Mechanistic derivation of the power law transmission function. arXiv 2008; 0809.1578..
Novozhilov, A., 2012. Epidemiological models with parametric heterogeneity: deterministic theory for closed populations. Math. Modell. Nat. Phenom. 7, 147–167.
Regoes, R.R., Ebert, D., Bonhoeffer, S., 2002. Dose–dependent infection rates of parasites produce the Allee effect in epidemiology. Proc. R. Soc. Lond. B Biol. Sci. 269, 271–279.

Smith, D.L., Dushoff, J., Snow, R.W., Hay, S.I., 2005. The entomological inoculation rate and Plasmodium falciparum infection in African children. Nature 438, 492–495.

Sneppen, K., Nielsen, B.F., Taylor, R.J., Simonsen, L., 2021. Overdispersion in COVID-19 increases the effectiveness of limiting nonrepetitive contacts for transmission control. Proc. Nat. Acad. Sci. 118, e2016623118.

Thompson, R.N., Hollingsworth, T.D., Isham, V., Arribas-Bel, D., Ashby, B., Britton, T., Challenor, P., Chappell, L.H.K., Clapham, H., Cunniffe, N.J., Dawid, A.P., Donnelly, C.A., Eggo, R.M., Funk, S., Gilbert, N., Glendinning, P., Gog, J.R., Hart, W.S., Heesterbeek, H., House, T., Keeling, M., Kiss, I.Z., Kretzschmar, M.E., Lloyd, A.L., McBryde, E.S., McCaw, J.M., McKinley, T.J., Miller, J.C., Morris, M., O'Neill, P.D., Parag, K.V., Pearson, C.A.B., Pellis, L., Pulliam, J.R.C., Ross, J.V., Tomba, G.S., Silverman, B.W., Struchiner, C.J., Tildesley, M.J., Trapman, P., Webb, C.R., Mollison, Restif, O., . Key questions for modelling COVID-19 exit strategies. Proc. R. Soc. B 287, 20201405.

Weitz, J.S., Park, S.W., Eksin, C., Dushoff, J., 2020. Awareness-driven behavior changes can shift the shape of epidemics away from peaks and toward plateaus, shoulders, and oscillations. Proc. Nat. Acad. Sci. 117, 32764–32771.

Wilson, E.B., Worcester, J., 1945. The law of mass action in epidemiology. Proc. Nat. Acad. Sci. 31, 24–34.

Wong, F., Collins, J.J., 2020. Evidence that coronavirus superspreading is fat-tailed. Proc. Nat. Acad. Sci. 117, 29416–29418.

Woolhouse, M.E.J., Dye, C., Etard, J.F., Smith, T., Charlwood, J.D., Garnett, G.P., Hagan, P., Hii, J.L.K., Ndhlovu, P.D., Quinnell, R.J., Watts, C.H., Chandiwana, S.K., Anderson, R.M., 1997. Heterogeneities in the transmission of infectious agents: Implications for the design of control programs. Proc. Nat. Acad. Sci. USA 94, 338–342.